RSC Advances

ROYAL SOCIETY OF CHEMISTRY

www.rsc.org/advances

Journal Name

ARTICLE

β-Cyclodextrin Modified Graphene Oxide-Magnetic Nanocomposite for Targeted Delivery and pH-sensitive Release of Stereoisomeric Anti-cancer Drugs

Received 00th January 20xx,
Accepted 00th January 20xx

DOI: 10.1039/x0xx00000x

www.rsc.org/

Congli Wang, Bo Li, Weifen Niu, Shasha Hong, Bassam Saif, Songbai Wang, Chuan Dong, Shaomin Shuang *

β-cyclodextrin modified graphene oxide-magnetic (MGC) nanocomposite as an innovative drug carrier was the first developed via an effective layer-by-layer-assembly method. Doxorubicin hydrochloride (DOX) and epirubicin hydrochloride (EPI) as model drugs were loaded onto the MGC via π–π stacking, hydrogen bond and hydrophobic interaction. The MGC exhibits remarkably higher loading capacity for DOX (909.09 mg/g) and EPI (781.25 mg/g) than magnetic graphene oxide (MG). The release profiles of drug are pH-sensitive which would control the release in acidic cytoplasm of cancer cells. Furthermore, cellular uptake using fluorescein isothiocyanate (FITC) labeled MGC proves successful internalization of MGC into the cytoplasm of MCF-7 cells. The fluorescence images demonstrate that MGC/DOX, to a certain extent, displays a more excellent delivery and superior release than MGC/EPI, due to the chiral select function of β-cyclodextrin (β-CD). The pure MGC shows no obvious cytotoxicity while drug loaded MGC reveals significantly high potency of killing MCF-7 breast cancer cells, suggesting that multi-functionalized MGC is an efficient nanoplatform for targeted delivery and controlled release of stereoisomeric anticancer drugs for biomedical applications.

1. Introduction

Graphene and its derivatives have attracted enormous attention due to their fascinating two-dimensional nanostructure consisting of a single layer of carbon atoms.[1-3] Among the derivatives, graphene oxide (GO) has abundant hydrophilic oxygen-containing groups (such as hydroxyl, carboxyl and epoxy) on its basal planes, which creates an opportunity to be functionalized for the preparation of versatile materials.[4] Multi-functionalized GO-based nanohybrids have especially aroused a rapidly increasing interest in variety of biomedical fields including biosensors,[5, 6] imaging,[7] scaffolds[8] and drug delivery,[9, 10] owing to their unique physiochemical properties of good biocompatibility and lack of obvious toxicity.[11, 12] The GO with a large specific surface area makes it a promising nanocarrier for drug delivery, which is available for enhancing the cellular uptake of small molecules.[13] The current developed drug carriers have plentiful virtues of prolonged blood circulation and drug solubilization. However, the therapeutic effect is mainly limited by lacking of targeted function to specific tumor sites and low degree of loading capacity. The targeting vehicle of high loading capacity is extremely desirable.

To reduce side effects and increase therapeutic efficacy, intensive research is ongoing to focus on the development of effective delivery systems to facilitate cellular uptake of drug and realize intelligent controlled release. A widely prescribed strategy to achieve efficient external targeting is to introduce various types of magnetic nanoparticles on the large surface of GO, which can drive the drug carriers to specific tumor tissues by a guided magnetic field.[14] A variety of magnetic nanoparticles including Fe_3O_4,[10] Co_3O_4,[15] Cu/Ni alloy,[16] Ni,[17] etc. have been successfully deposited on the basal plane of GO by physical or chemical methods. However, it's relatively hard to control the size distribution, deposition density and morphology of the as-prepared magnetic nanoparticles. Magnetic Fe_3O_4 has a great deal of advantages over other magnetic nanoparticles such as strong superparamagnetism, low toxicity, excellent biocompatibility and easy preparation process.[18] The immobilization of Fe_3O_4 on the platform of GO can not only avoid aggregating of Fe_3O_4 nanoparticles but also protect them from oxidation. Unfortunately, the hydrophilic groups of GO are easy to lost by heating during the process of in situ deposition of metallic salts, affecting further dispersion and loading amount of the nanocomposites.[19] The further functionlization of magnetic graphene oxide (MG) is essential for applicable purpose.

Various efforts have been made to explore potential applications of MG in drug delivery systems. Yang's group firstly developed superparamagnetic graphene oxide–Fe_3O_4 nanoparticles and conjugated the MG with folic acid for loading doxorubicin hydrochloride (DOX).[10, 20] In order to improve the biocompatibility, a series of polymers, such as

Department of Chemistry and Chemical Engineering and Institute of Environmental Science, Shanxi University, Taiyuan 030006, P. R. China. E-mail: smshuang@sxu.edu.cn; Fax: +86-531-7018842; Tel: +86-531-7011688

polyethylene glycol (PEG),[21] chitosan (CHI),[22] polyethylenimine (PEI),[23] poly[2-(dimethylamino) ethyl methacrylate] (PDMAEMA),[24] and so on, were employed to modify MG for loading and release of DOX and levofloxacin. However, relative low loading capacity and complicated manipulated process have confined further use. The drug delivery systems are facing a great challenge toward high effective loading. Recently, Qiu et al. firstly introduced β-cyclodextrin (β-CD) to graphene oxide-magnetic nanohybrid as a novel stationary phase for efficient enantioseparation of tryptophan.[25] Yan and Liu et al. fabricated β-CD functionalized magnetic graphene nanocomposite as an adsorbent for the removal of organic dyes[26] and heavy metal ions.[27] These researches inspire us and motivate us to try to expand such a nanocomposite for durg delivery.

DOX and epirubicin hydrochloride (EPI) (illustration in Scheme. 1) as stereoisomers of anthracycline-based broad-spectrum antitumor drugs, play an important role in restraining the composition of nucleic acids of cancer cells.[28] Only when the drugs are sufficiently migrated inside the cancer cells will it operates. However, most of the drug vehicles could neither be transported into the cell due to the large size nor show adequate release of the drug in cytoplasm,[29] resulting in a very low internalization of drug and poor effect of chemotherapy. The combination of β-CD and MG as the drug vessel possesses not only the unique inclusion properties of β-CD but also loading and magnetic targeting capacities of MG, which provides an admirable opportunity for targeted drug delivery.

Herein, a targeted delivery carrier of β-cyclodextrin modified graphene oxide-magnetic nanohybrid were successfully fabricated. β-CD was assembled onto the surface of MG by hydrophobic, van der Waals and hydrogen bonding interactions. DOX and EPI were used as model drugs to assess the drug-loading and releasing properties and the effect of pH was examined. Cell cytotoxicity and cellular imaging were carried out toward further application. It will be expected that this nanocarrier has a great potential in targeted delivery, controlled release and biomedical applications.

2. Experimental

2.1 Materials

Graphite powder, sodium chloride (NaCl) and sodium nitrate ($NaNO_3$) were purchased from Tianjin Hengxing Chemical Reagent Manufacturing Co. Ltd. (Tianjin, China). Iron chloride tetrahydrate ($FeCl_2•4H_2O$) and ferric chloride hexahydrate ($FeCl_3•6H_2O$) were bought from Tianjin Guangfu Fine Chemical Industry Research Institute (Tianjin, China). β-CD was obtained from Guangdong Yunan Cricoid Dextrin Factory and purified using recrystallization (Guangdong, China). DOX and EPI were purchased from Dalian Mellon Biological Technology Co. Ltd. (Dalian, China). All the other chemicals used were analytical grade without any further purification. Deionized water was prepared by a Simplicity ®UV system (Millipore Corporation, France) and used during the whole experiments.

2.2 Characterization

Fourier transform infrared (FTIR) spectra were obtained with a Shimadzu FTIR-8400s spectrometer using KBr discs in the 400-4000 cm^{-1} region (Shimadzu, Japan). The morphology and size of the samples were recorded on a Tecnai G^2 20 transmission electron microscopy (TEM) (FEI Hong Kong co., LTD, China). A Dimension® Icon® (Bruker Nano, Inc., Santa Barbara, CA, USA) with a tapping mode is used to obtain the atomic force microscopy (AFM) images to characterize the thickness of the prepared nanohybrids. X-ray powder diffraction (XRD) was carried out on a Rigaku MiniFlex Ⅱ diffractometer with Cu-Kα radiation and at a scanning speed of 4 °/min (Rigaku, Japan). The magnetization curve of the nanohybrid was measured on a Lakeshore vibrating sample magnetometer (VSM) at room temperature (American Lakeshore). Thermogravimetric analysis (TGA) was collected on a Rigaku Thermo Plus Evo TG 8120 instrument at a heating rate of 10 °C/min from room temperature to 800 °C under N_2 flow (30 mL/min) (Rigaku, Japan). UV–vis absorption spectra were obtained using a Hitachi U-2910 UV-Vis spectrometer (Hitachi, Japan). Fluorescence measurements were performed on a Hitachi F-4500 fluorescence spectrophotometer (Hitachi, Japan).

2.3 Preparation of MGC nanoparticles

2.3.1 Preparation of GO. GO was prepared from natural graphite powder using a modified Hummers method.[30] In brief, graphite powder was oxidized with strong oxidants, including concentrated H_2SO_4, $KMnO_4$, $NaNO_3$ and 30% H_2O_2, under vigorous stirring. The resulting mixture was further centrifuged at 4000 rpm for 10 min, and washed with 5% hydrochloric acid and deionized water several times respectively, until the pH of the supernatant was neutral. To synthesis oxidized graphene, the products were sonicated for 1 h, followed by centrifuging to remove unexfoliated GO. Then the sample was dried under vacuum at 50 °C for 24 h.

2.3.2 Preparation of MG. The magnetic Fe_3O_4/GO nanohybrid was prepared by the chemical precipitation method[25]. Firstly, GO was sonicated in deionized water for several hours, followed by placed in a three-necked flask and heated to 80 °C. The flask was then purged with N_2 for 30 min. After that, $FeCl_3•6H_2O$ and $FeCl_2•4H_2O$ were added into the flask with vigorous mechanical agitation at the protection of N_2. Then, $NH_3•H_2O$ was added to the mixture dropwise until the pH of the solution was approximately 10. The reaction was kept stirring at 80 °C for another 40 min. After cooling to room temperature, the mixture was magnetically separated and washed with double-distilled water and anhydrous ethanol. Finally the prepared products named as MG1 were dried under vacuum and obtained for further usage. Other products (MG2 and MG3) with different weights were then prepared according to the above method (Table1).

2.3.3 Synthesis of MGC. To conjugate MG nanohybrid with β-CD, β-CD solution was added to MG1 suspension liquid (m_{MG1}: $m_{β\text{-}CD}$=1:10) under N_2 atmosphere. After vigorous stirring, the

three-necked flask was heated to 65 °C and maintained 4 h in water bath.[31] The resulting substance named as MGC1 was collected by an additional magnet, washed with anhydrous ethanol for several times to remove excess-β-CD, and dried in a vacuum at 40 °C overnight. By adding different quality of β-CD,

Table 1 The weight ratio of feed amount and grafting content of β-CD determined by TGA

MG Sample	m_{GO}: m_{FeCl3}	MGC Sample	m_{MG}: $m_{\beta\text{-}CD}$	β-CD wt %
MG1	1:10	MGC1	1:10	9.12
		MGC2	1:20	9.69
		MGC3	1:30	9.24
MG2	1:20	MGC4	1:10	14.08
		MGC5	1:20	21.18
		MGC6	1:30	15.25
MG3	1:30	MGC7	1:10	8.73
		MGC8	1:20	9.81
		MGC9	1:30	9.2

other samples (MGC2–9) with various weights were then prepared using the same approach (as shown in Table1).

2.4 Drug loading and release

2.4.1 Loading of drug onto MGC1-9 and MG1-3. The drug loading capacity of MGC1-9 was determined by adding different amount of DOX or EPI to fixed concentration MGC nanohybrid and then mixed thoroughly. The suspension was put on the HY-4 speed-governing multi-purpose oscillator and incubated at room temperature for 3 days in the dark. As a comparison, MG1-3 was loaded with DOX or EPI under the similar conditions. After that, the resulting MGC and MG with DOX or EPI were collected by magnetic separation and filter membrane. The concentration of DOX or EPI in the supernatant was determined using the UV-Vis absorbance calibration curve according to the measurement of a series of concentrations of drug solutions at 478 (DOX) or 494nm (EPI). The drug loading capacity of MGC1-9 and MG1-3 was calculated according to the following formula (Eq. (1)):

$$\textbf{Drug loading capacity} = \frac{\mathbf{M_{the\ initial\ amount\ of\ drug} - M_{the\ residual\ amount\ of\ drug}}}{\mathbf{M_{the\ amount\ of\ carrier}}} \quad \textbf{(1)}$$

2.4.2 Release behaviors of MGC/DOX and MGC/EPI. The release of drug-loaded MGC was carried out by adding MGC/DOX or MGC/EPI into phosphate-buffered saline (PBS, 0.1 M) at pH 5.30 (the cytoplasm pH of cancer cells) and 7.40 (the physiological pH) at 37 °C. The release behavior was kept under constant stirring, and quantitative solution was taken out for fluorescence measurement at a series of time points. The concentration of DOX or EPI released from MGC4-6 was measured by fluorimetry at the wavelength number of 588 (DOX) or 591 (EPI) nm using a calibration curve prepared under the same condition. The percentage of drug released was given as the following equation (Eq. (2)):

$$\textbf{The percentage of drug released} = \frac{\mathbf{M_{the\ released\ amount\ of\ drug}}}{\mathbf{M_{the\ loading\ amount\ of\ drug}}} \times \mathbf{100\%} \quad \textbf{(2)}$$

2.5 Cellular uptake and drug release in cell

Cell uptake studies were carried out by MCF-7 cells, a human breast cancer cell. The MCF-7 cells were cultured in 24-well plates in RPMI-1640 medium in a fully humidified incubator. The media were supplemented with 10% fetal bovine serum (FBS) and 1% penicillin-streptomycin at 37 °C containing 5% CO_2. The nanocarrier was labeled by adding fluorescein isothiocyanate (FITC) to MGC and vibrating overnight. The FITC labeled MGC5 (MGC/FITC) was centrifuged and washed for 3 times. Then MCF-7 cells were incubated with pure MGC, MGC/FITC, MGC/DOX and MGC/EPI with the final concentration of 20 μg/mL at 37 °C. Finally the incubated MCF-7 cells were washed with PBS and the cellular uptake and drug release were performed with a FV1000 confocal laser scanning microscope (CLSM) (Olympus Co., Ltd. Japan).

2.6 Cytotoxicity of MGC/DOX and MGC/EPI to MCF-7 cells

To research the in vitro cytotoxicity of MGC/DOX and MGC/EPI towards tumor cells, standard MTT assays were carried out by MCF-7 cells. Briefly, the MCF-7 cells were plated into 96-well cell-culture plates at a density of 1×10^4 cells per well and grown overnight at 37 °C under 5% CO_2. Then, the cells were incubated with various concentrations of MG, MGC, MGC/DOX and MGC/EPI in a fully humidified atmosphere for a further 24 h. The relative cell viability was checked by the MTT assay according to the manufacturer suggested procedures.

3. Results and discussion

3.1 Preparation and characterization of MGC nanoparticles

The preparation strategy of the MGC was shown in Scheme 1. Firstly, GO was prepared by a modified Hummer's method[30]. Then the MG nanocomposites were synthesized by a simple in situ deposition. In order to improve the water solubility and increase the amount of drug loading, β-CD was modified on the surface of MG through hydrogen bond and hydrophobic interaction. Thus, MGC with superparamagnetism and high loading capacity was obtained.

To demonstrate the morphology and size of as-prepared nanohybrid, representative TEM was used to characterize the surface morphologies. As shown in Fig. 1, it is obvious that graphite powder has been exfoliated into thin flakes of GO after oxidation (Fig. 1b). The pure Fe_3O_4 nanoparticles are seriously gathered for clusters and the particle diameter significantly increases, which is disadvantageous for drug delivery (Fig. 1a). After Fe_3O_4 is immobilized on the surface of GO, it is found that a large amount of uniform Fe_3O_4 nanoparticles with average size of about 13±1.2 nm are distributed on the surfaces and edges of the GO nanosheet,

which is necessary to keep a powerful magnetism (Fig. 1c). Furthermore, no great aggregation of Fe_3O_4 or large blank on GO is observed, and almost no unbonded Fe_3O_4 is viewed outside of GO sheets. It is noted that the morphology of MG shows no significant difference from GO, unambiguously indicating that this moderate method would not damage the layered structure during the functionalized process. After the modification of β-CD, it can be clearly observed that

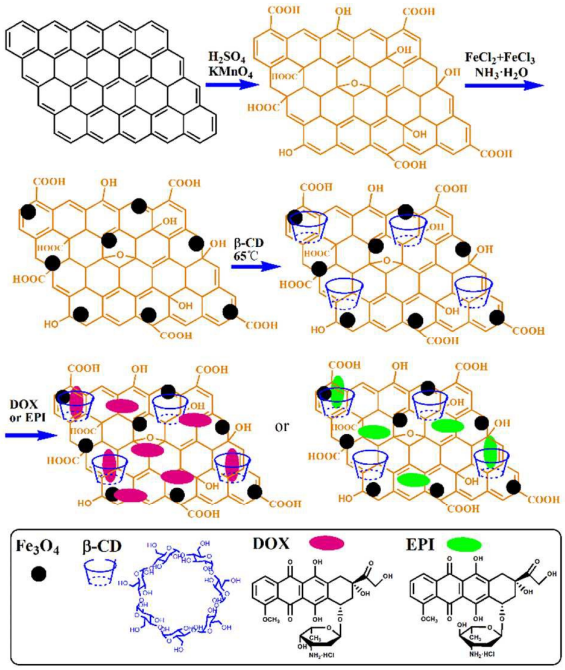

Scheme. 1 The preparation of β-CD-functionalized magnetic graphene oxide (MGC) and representation of loaded with DOX and EPI.

GO is the matrix of Fe_3O_4 nanoparticles and the β-CD is covering on the surface, like a film,[32] which may be important to improve the water solubility of the carrier. The TEM images could provide direct evidence for the successful fabrication of MGC nanocomposites. In AFM images (Fig. S1, ESI†), GO reveals a height of 1.0 nm, suggesting a single layer graphene oxide sheet.[33] After functionalization of Fe_3O_4 and β-CD, an obvious increase of thickness is observed, mainly due to the attachment of Fe_3O_4 and β-CD on both planes of GO.

The loading behaviors of DOX or EPI on the nanocarriers were determined by UV-Vis spectrophotometer. As displayed in Fig. 2A and B, the specific UV-Vis peaks at 252, 290 and around 485 nm are attributed to absorption of DOX (Fig. 2A(a)). The broad peaks at 253 and 298 nm are ascribed to the characteristic

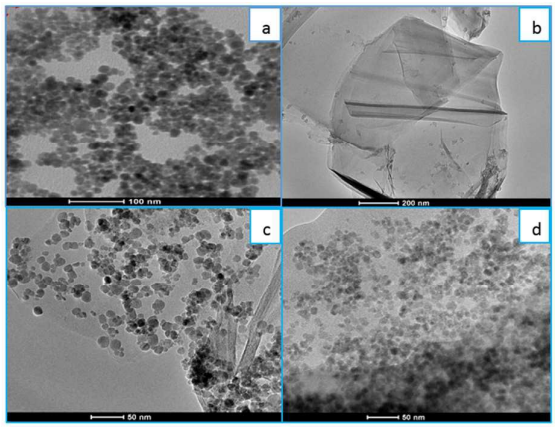

Fig. 1 TEM images of Fe_3O_4 (a), GO (b), MG (c) and MGC (d).

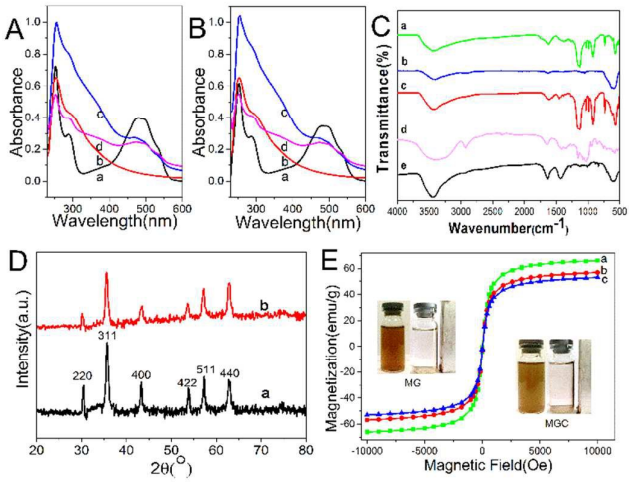

Fig. 2 (A) UV-Vis absorption spectra of DOX (a), GO (b), MG/DOX (c) and MGC/DOX (d). (B) UV-Vis absorption spectra of EPI (a), GO (b), MG/EPI (c) and MGC/EPI (d). (C) FTIR spectra of GO (a), Fe3O4 (b), MG (c), β-CD (d) and MGC (e). (D) XRD patterns of MG (a) and MGC nanocomposite (b). (E) Magnetic hysteresis loops of the prepared Fe3O4 (a), MG (b) and MGC (c). Inset: the upper is MG and the under is MGC, the insets show the photographic pictures of the MG and MGC hybrid in the absence (left) and presence (right) of an external magnet. Note: The MG is on behalf of MG2, and MGC is representative of MGC5.

absorption of GO (Fig. 2A(b)). After MG and MGC are loaded with DOX, the characteristic absorbance peak at 485 nm presents and the peak around 252 nm shifts to 255 nm, which are corresponded to the peak of free DOX, demonstrating that DOX molecule has been successfully loaded onto MG and MGC (Fig. 2A(c) and (d)). DOX and EPI have stereoisomeric structure with the same absorption peak, so the similar characteristic absorption peaks have been observed in both EPI, MG/EPI and MGC/EPI as shown in Fig. 2B(a), (c) and (d), indicating that EPI can also be loaded on the nanocarrier.

To further characterize the formation of GO, MG and MGC, corresponding FTIR spectra were shown in Fig. 2C. As expected, the spectrum of GO is quite fit in with previous work.[34] GO with the layered structure has a lot of oxygen-containing functional groups located on its basal planes and

around the sheet edges, including hydroxyl, epoxy and carboxylic acid groups.[35] The broad, intense band at 3435 cm^{-1} is attributed to the stretching of O-H (Fig. 2C(a)). The characteristic band at 1741 cm^{-1} is ascribed to the C=O of carboxylic groups which is shifted to 1610 cm^{-1}, indicating the formation of the -COO- group after modifying with Fe_3O_4 (Fig. 2C(c)). The peak at 1633 cm^{-1} is corresponding to the stretching of C=C. The bands at 1267 cm^{-1} and 1033 cm^{-1} are associated with the stretching vibrations of C-OH and the deformation vibrations of C-O, respectively (Fig. 2C(a)). For MG, the FTIR spectrum is different from GO as evidenced by the appearance of an intense peak at 579 cm^{-1}, which belongs to the stretching vibration of Fe-O bond. Moreover, the Fe-O stretching peak has shifted to higher wavenumbers compared to that of 569 cm^{-1} in bulk Fe_3O_4 (Fig. 2C(b)), demonstrating that GO has been successfully functionalized with Fe_3O_4 nanoparticles.[36] After MG nanohybrid is further modified with β-CD, it could be observed that the FTIR spectrum of the MGC exhibits characteristic absorbing peaks of β-CD. The band at 1161 cm^{-1} is assigned to the coupled C-O-C stretching/O-H bending vibrations. The featured peaks at 1010 cm^{-1} and 1076 cm^{-1} is attributed to the coupled C-O/C-C stretching/O-H bending vibrations, and the C-H/O-H bending vibration is at 1429 cm^{-1} (Fig. 2C(d) and (e)). The above results demonstrate that β-CD has been anchored on the surface of MG successfully.

To prove the deposition of Fe_3O_4 on the surface of GO and the crystal structure of MG and MGC, the XRD patterns of MG and MGC nanocomposite are presented in Fig. 2D. The diffraction peaks of the as-prepared MG nanoparticles at 2θ=30.31º, 35.58º, 43.19º, 53.58º, 57.18º and 62.87º are corresponding to the (220), (311), (400), (422), (511) and (440) planes of magnetite respectively, which is consistent with the cubic spinel crystal Fe_3O_4 according to the Joint Committee On Powder Diffraction Standards (JCPDS) Card no. 89-3854.(Fig. 2D(a)).[37, 38] As compared with MG nanocarrier, the MGC nanocomposites display all diffraction peaks of Fe_3O_4 (Fig. 2D(b)), and no obvious shifts can be observed, indicating that Fe_3O_4 nanoparticles have been successfully connected with GO and have no effect on the layered structure during all the experimental processes. What's more, the average particle size of Fe_3O_4 could be estimated to be 14 nm by the formula of Scherrer, which is in accordance with the data measured from the TEM images (Fig. 1c).

The magnetic properties of MGC nanohybrids were investigated at room temperature on a VSM. As shown in Fig. 2E, the magnetic hysteresis loops of all the samples display S-like curves. The values of specific saturation magnetization (Ms) of Fe_3O_4 (Fig. 2E(a)), MG (Fig. 2E(b)) and MGC (Fig. 2E(c)) are 65.79, 57.25 and 55.64 emu/g, respectively. It is evident that the MG possesses good magnetic property while the Ms of MG is weaker than Fe_3O_4, implying that Fe_3O_4 has been successfully in situ deposited on the surface of the GO. The Ms of MGC has a slight decrease for MG, which is likely ascribed to the absorption of β-CD leading to a decrease of the relative content of Fe_3O_4 in the nanohybrid. Furthermore, the magnetization curves have no coercivity and remanence, indicating that there is no remaining magnetization. The insets of Fig. 2E demonstrate that once an external magnetic field is applied, the uniform and rufous suspension of MG and MGC could be attracted quickly toward the magnet, giving rise to the solution clear and transparent. These results reveal that both MG and MGC exhibit excellent superparamagnetic behavior and could be used for targeting drug delivery.

TGA was further used to investigate the amount of β-CD conjugating on the surface of MG. A series of MG and MGC nanocomposite were prepared by the chemical deposition and "grafting to" way. As shown in Table 1, MG1-3 were synthesized with different feed amounts of $FeCl_3$ and $FeCl_2$ by the same component, and MGC1-3 were prepared by the same MG1 with different feed quantities of β-CD. Thus, products MG1-3 have the same GO but different content of Fe_3O_4, and the generated MGC1-3 or MGC4-6 or MGC7-9 should have the same MG but different content of β-CD. Fig. 3 displays the thermal behaviors of MG and MGC nanohybrid. As shown in Fig. 3, a slow weight loss at low temperature (<100 °C) is observed, which can be assigned to the loss of residual solvent and water. Another stage of weight reduction occurs below 220 °C, indicating the removal of the labile oxygen-containing functional groups on GO and Fe_3O_4.[39] It is found that the weight reduction region at about 280 - 600 °C could be attributed to the decomposition of β-CD, and the significant weight loss in the high-temperature region (about 600 - 800 °C) belongs to the breakdown of GO skeleton.[31] Thus, the amount of β-CD molecules could be determined as exhibited in Table 1, demonstrating that large amount of β-CD has been adsorbed on the surface of MG. In table 1, feed amount means added amount and grafting content means modified content. We notice that the feed amount of β-CD on MGC3, MGC6 and MGC9 with the ratio 1:30 is greater than that on MGC2, MGC5 and MGC8 with 1:20. While modified content for MGC3, MGC6 and MGC9 is lower than that on MGC2, MGC5 and MGC8. The phenomenon may be interpreted as that the modified content of β-CD is mainly related to the efficient surface area of MG. When the feed amount of β-CD is saturated, the grafting amount is optimal. When excessive β-CD is added, the grafting content shows a slight decline due to the existence of space steric hindrance and site competition between molecules in the dynamic process, which is the opposite of rise theoretically. So the MGC5 shows the highest modified amount of β-CD. This is a fascinating result that MG nanohybrid could graft many β-CD molecules, which may provide a good opportunity to load more drugs (the following data will reveal this point). As a comparison, the TGA of MG3 has also been investigated, as shown in Figure 3C. It is clear that MGC exhibits the much higher thermal stability than MG below 200 °C, which offers a better protection for Fe_3O_4.

3.2 Drug loading and in vitro release

Aromatic molecules including abundant anticancer drugs could be loaded on the surface of sp^2-carbon nanomaterials, particularly GO.[40] DOX and EPI, as drug models, were loaded onto the surface of MG2 and MGC5 by a simple mixture and

vibrating approach via π–π stacking and hydrophobic interactions between functionalized GO and drugs. The free drug was removed by a filter membrane and the loading efficiency of the carrier was calculated via quantifing the concentration of supernatant using UV–Vis spectrophotometer. As shown in Fig. 4A, the absorbance of DOX is reduced by 84% with the MGC5 while only a 68% decrease is observed for MG2, indicating a higher efficient loading on MGC than MG. The data of EPI were obtained in a parallel way and similar results have been observed. As expected, the absorbance of EPI in Fig. 4B shows a significant reduction of 74% for MGC5 while only a 56% decline in MG2 is observed. These results demonstrate that more DOX than EPI could be adsorbed on the nanocarrier of MGC, likely due to the space block caused by the stereoisomerism.

To investigate the effect of pH on the drug loading of MGC5, the same concentration of MGC5 and DOX or EPI were incubated in different PBS (0.1 M, pH=2.0-7.0) and the unbound drugs were isolated with a filter membrane. The difference of absorption between pure drug and supernatant fluid is the

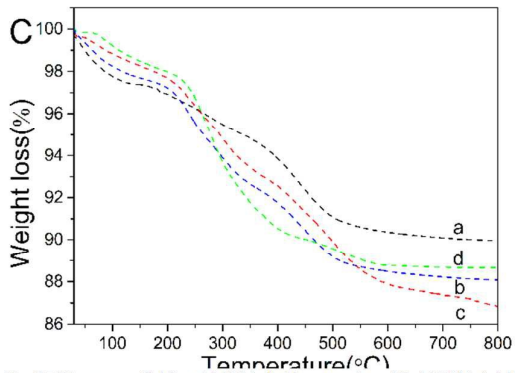

Fig. 3 TGA curves of MG and MGC hybrid composites, (A): MGC1 (a), MGC2 (b) and MGC3 (c). (B): MGC4 (a), MGC5 (b) and MGC6 (c). (C): MG3 (a), MGC7 (b), MGC8 (c) and MGC9 (d).

amount of drug loaded by the carrier. As shown in Fig. 4C, it can be observed that the loading capacity of MGC5 for DOX and EPI rises gradually from pH 2.0 to 6.0 and increases dramatically at pH 7.0, whereas, the loading capacity decreases greatly when the pH is greater than 7.0. The loading experiment is a dynamic equilibrium process.[41] In an acidic or basic environment, the lower or higher pH could cause high degree of protonation of DOX and EPI, resulting in the partial dissociation of hydrogen bonding[42, 43] and the loading capacity is not behaving well. At pH 7.0, multiple strong hydrogen-bonding interactions between -OH, -COOH in MGC and -OH, -NH_2 in drugs are conducive to the incorporation of MGC and drugs, leading to a rapid increase of loading amount.[42, 44] As a result, the subsequent experiments

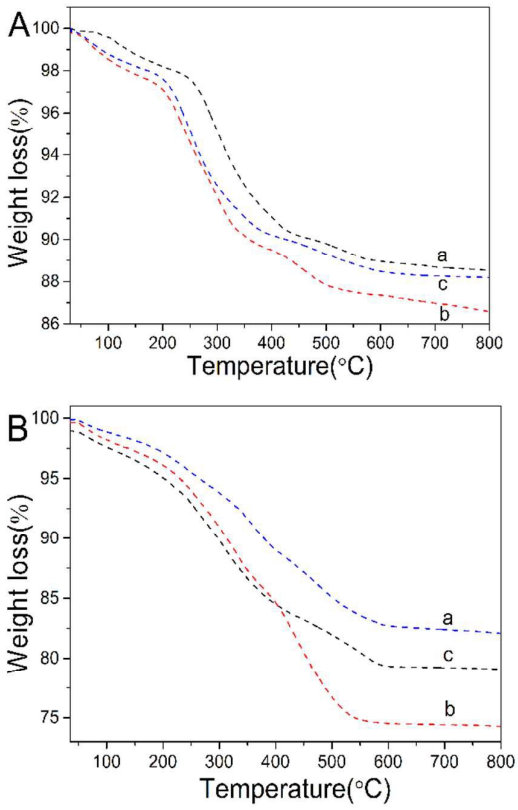

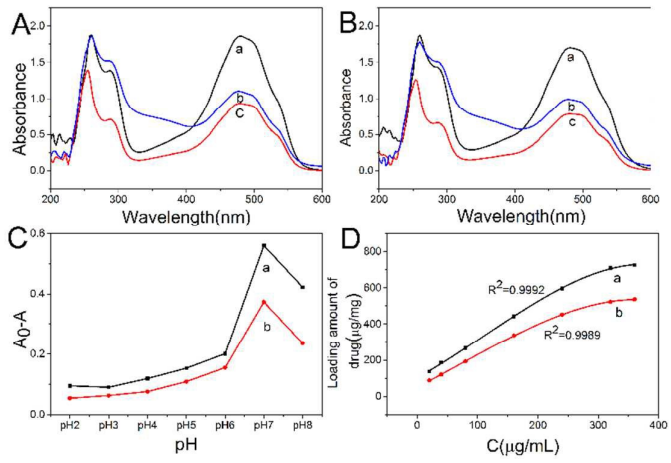

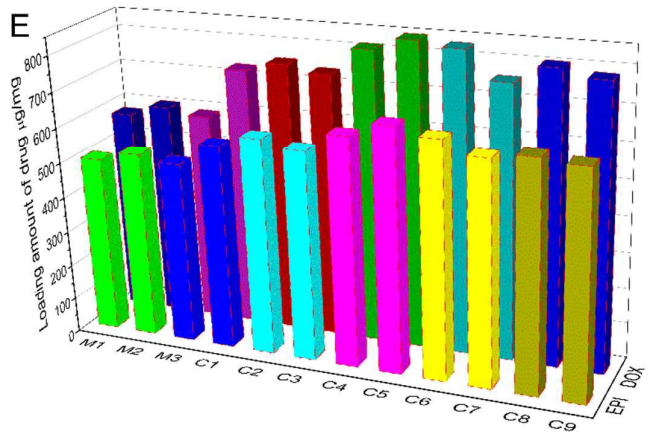

Fig. 4 (A/B) UV-Vis absorbance spectra of DOX (A) and EPI (B) of pure drug (a), supernatant of MG (b) and MGC (c) after adding drug. (C) The influence of pH on loading capacity of MGC for DOX (a) and EPI (b) (A_0: UV-Vis absorbance intensity of pure DOX and EPI, A: UV-Vis absorbance intensity of supernatant after DOX and EPI adsorbed on MGC). (D) The adsorption Equilibrium isotherm of DOX (a) and EPI (b) by MGC. (E) Loading amount of MG and MGC for DOX (back row) and EPI (front row). Note: M is short for MG, MGC is referred to as C.

are operated at pH 7.0. With a large specific surface and hydrophobic cavity, MGC is supposed to have excellent loading behavior. To determine the saturated level of DOX and EPI loaded on MGC5, different amounts of DOX or EPI were added into the carrier solution of fixed concentration at pH 7.0. After removal of free DOX, as shown in Fig. 4D(a), it is found that the loading capacity of MGC5 for DOX increases with the increasing initial DOX concentration, and it reaches 720 μg/mg when the initial DOX concentration is 360 μg/mL, which is still unsaturated. For EPI, similar tend can be observed in Fig. 4D(b), and the loading amounts of EPI increase from 92 to 509 μg/mg which is less than DOX. Through curve fitting of Langmuir isothermal adsorption, it is found that the maximum adsorption capacities of MGC5 for DOX and EPI are 909.09 and 781.25 mg/g respectively (Table 2), considerably higher than the previously reported values.[45, 46]

In order to study the influence of the content of β-CD on drug loading, the loading amounts of MG1-3 and MGC1-9 for DOX and EPI under the same conditions are also presented for comparison in Figure 4E. It states clearly that the carriers of MG1-3 possess a low ability about 600 and 500 μg/mg for DOX and EPI loading, while MGC1-9 have a loading capacity of almost 850 and 700 μg/mg for DOX and EPI, nearly 1.5 times that of MG, indicating that β-CD is responsible for much more drug loading. As shown in Fig. 4E and Table 1, the variation tendency of drug loading is in a good agreement with the content of β-CD. In addition, the loading amounts of MGC5 is the largest among the above nanocarrier due to the greatest content of β-CD. These results reveal that the MGC nanocarrier could load of DOX and EPI with exceptionally high loading amounts. Thereby, this nanocarrier could be a potential vehicle for highly efficient load and delivery of DOX or EPI, and MGC5 is chosen for the following experiments.

In addition, to further obtain the distribution of adsorption molecules with more reliability when the adsorption process reaches to an equilibrium state, the adsorption isotherms are built and compared with the common isotherm models of Langmuir (Eq. (3)) and Freundlich (Eq. (4)), as follows:

$$\frac{C_e}{Q_e} = \frac{C_e}{Q_m} + \frac{1}{Q_m K_L} \quad (3)$$

$$Q_e = lnK_f + \frac{1}{n} lnC_e \quad (4)$$

It is well known that the Langmuir model is basically used for monolayer adsorption on a surface with a homogeneous system, while the Freundlich model is suitable for multilayer adsorption of a heterogeneous system.[47] In order to assess different isotherms models, the fitted plots from the two isotherms are shown in Fig. 5 with the experimental data for adsorption of DOX or EPI onto the nanocarrier of MGC, and the values of parameters for the two models are revealed in Table 2. As shown in Table 2, by comparison of linear correlation coefficients (R^2), it is found that the Freundlich model is a better fit for the experimental results of drug loading than the Langmuir model, indicating a multilayer adsorption.

It is reported that this type of nanocarrier could be taken up by tumor cells via the endocytosis at the physiological pH of 7.4, while it declines to an acidic pH value nearly 5.3 in endosomes and lysosomes.[48] For purpose of enhancing the efficient release of the anti-cancer drug inside the tumor tissue or cells and avoiding undesired release during the delivery process in blood circulation, it's significant for the release of drug from the carrier to be pH-responsive. Thus, the drug-release behaviors of MGC/DOX and MGC/EPI were performed at pH 5.3 and 7.4 at

Table 2. The adsorption isotherm parameters of MGC for DOX and EPI

Models	Langmuir Isotherm			Freundlich Isotherm		
Drug		DOX	EPI		DOX	EPI
Adsorption Parameters	q_m	909.09	781.25	n	2.1354	1.6929
	K_L	0.01123	0.0150	K_f	49.472	18.733
	R^2	0.9062	0.9236	R^2	0.9648	0.9843

Note: The unit of q_m, K_L and K_f is mg/g, mL/mg and mL/g, respectively.

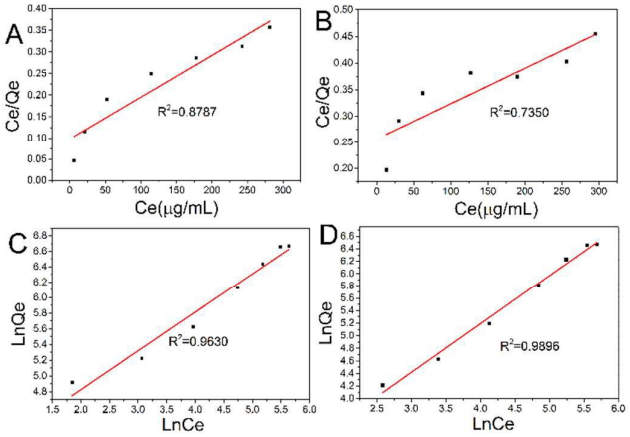

Fig. 5 (A/B) The Langmuir Isotherm linear dependence of Ce/Qe on Ce for the adsorption of DOX (A) and EPI (B) on MGC. (C/D) The Freundlich Isotherm linear dependence of LnQe on LnCe for the adsorption of DOX (C) and EPI (D) on MGC.

37 °C. At various time points, quantitative solutions were taken out and the supernatants were determined by fluorescence measurement. As shown in Fig. 6, at neutral PBS (pH 7.4) to simulate normal physiological condition, the DOX and EPI are released from MGC nanohybrids in a very slow fashion and only below 18% (DOX) and 15% (EPI) of the total bound drugs are released for 50 h, which can be interpreted as that the stronger hydrogen bonding interactions results in a slower and inefficient release. However, in acidic conditions, the release of DOX and EPI from MGC rises dramatically within the first 10 hours and then levels off gradually from 10 to 50 h. The maximum cumulative release of DOX and EPI are about 60% and 35% at pH 5.3 within 50 h, due to the weak hydrogen-bonding interactions between the –OH and –COOH groups on MG and –OH and $–NH_2$ groups in DOX or EPI. The release includes two parts, one is from the desorption of the surface-bound drug molecules on MGC surface,[49] another is from the gradual release of drug molecules which have been entrapped in β-CD cavities.[50] The complete release of drugs couldn't be achieved at either pH, owing to the diffusion equilibrium between MGC/drug inclusion complexes and the released drug which would inhibit the complete drug release.[51] Furthermore, for the steric hindrance of EPI is much higher than DOX, under the same condition, more EPI will remain entrapped in the cavity of β-CD and less EPI than DOX would be released from the MGC carrier. In addition, drug release behaviors are in complete agreement with the loading amounts and the content of β-CD, suggesting that the conjugation of β-CD is conducive to the release of drug. It is well known that the microenvironments in extracellular tissues of tumors and intracellular lysosomes and endosomes are acidic, so pH-responsive drug release from MGC is advantageous to the clinical therapy of cancer.[52] As an ideal delivery vehicle, the DOX and EPI can be transported to the targeted site by the water-dispersive MGC, then the drug payload could be internalized to cancer cells through endocytosis. In the acidic microenvironments (pH is about 5.3),

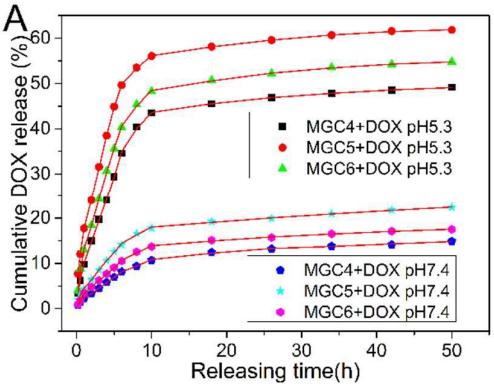

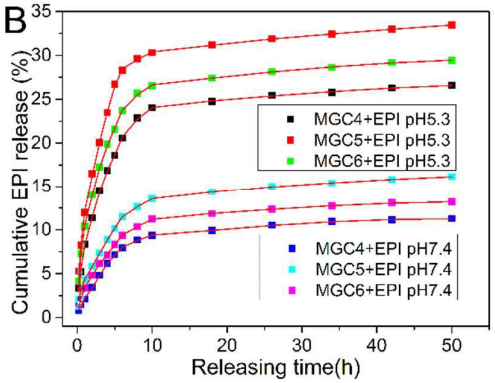

Fig. 6 Cumulative release of DOX (A) and EPI (B) from MGC/DOX and MGC/EPI nanoparticles at pH 5.3 and 7.4.

protonation of $-NH_2$ groups in DOX or EPI molecules can lead to a positive charge to weaken the part of the hydrogen bond interactions between drugs and the nanocarrier MGC, triggering more desired drug release. Considering the different pH-sensitivity release behaviors of DOX and EPI from MGC, the multi-functionalized nanohybrid MGC could be served as an excellent candidate for intelligent drug release to satisfy different needs.

3.3 Cellular uptake, drug release and cytotoxicity

To further confirm the MGC nanocarrier can transport DOX or EPI to the targeted site, and especially can effectively release the drugs in the cell, pure MGC, MGC/FITC, MGC/DOX and MGC/EPI of equivalent concentration were incubated with the MCF-7 cells for 2 h. The intracellular distribution of the MGC nanocarrier with or without drug was examined by a CLSM. As shown in Fig. 7A, the MCF-7 cells treated with blank MGC shows no obvious fluorescence, while strong green fluorescence signals throughout the entire cell cytoplasm could be observed in the cells after incubation with MGC/FITC, giving evidence for the successful internalization of MGC. To understand the release behavior of DOX or EPI from MGC, the MCF-7 cells were incubated with the same concentration of MGC/DOX and MGC/EPI for a series of time. As shown in Fig. 7B(a), the fluorescence intensity in cytoplasm of the MCF-7 cells treated with MGC/DOX increases dramatically with the growth of time, proving the effective cellular internalization of MGC nanocarrier. After 8 h treatment, the fluorescence especially in nucleus rises gradually, suggesting the slow and efficient release of DOX from MGC. This can be interpreted as that the large specific surface of MGC nanocarrier is internalized into cells by endocytosis followed by that free DOX quickly migrates into nucleus, so that DOX can only move into the cell nucleus after slow release from MGC. For the cells treated with MGC/EPI, similar fluorescence growth trend could be observed (Fig. 7B(b)), however, much stronger fluorescence is found in the MCF-7 cells after incubation with MGC/DOX than that with MGC/EPI, demonstrating more release and cell uptake of DOX under acidic condition, which is consistent with the release in vitro. It reveals that the more DOX than EPI can be rapidly and effectively transported to the targeted tumor

cells by multi-functionalized MGC. Thus, it can be concluded that MGC/DOX and MGC/EPI could be efficiently taken up by MCF-7 cells accompanying abundant intracellular release, followed by migrate DOX or EPI into the cell nucleus while the nanocarrier is left in cell cytoplasm. These fascinating properties give a great opportunity for MGC nanocarrier to be a potential candidate for targeted delivery and controlled release of DOX and EPI for cancer treatment.

The following work confirms the anti-tumor efficacy of MGC/DOX and MGC/EPI, for this purpose, MCF-7 cells were incubated with MGC/DOX and MGC/EPI in concentrations of 1 to 20 μg/mL for 24 h. The cell viability was determined by standard MTT assay, as shown in Fig. 7C(c) and (d), the dose-dependent cell viability for both MGC/DOX and MGC/EPI decreases with increasing carrier concentrations. Furthermore, at each concentration, the cytotoxicity of MGC/DOX is remarkably higher than that of MGC/EPI, likely due to the different release behaviors of the carrier.[53] The results reveal that the MGC loaded of DOX or EPI has the potential for killing MCF-7 cells. As a control, the pure MG and MGC were carried out with the protocol described above, suggesting that the cell viability of pure MG decreases gradually with the increment of the concentration of MG (Fig. 7C(b)). Whereas, it is worthy of note that no obvious toxicity is found at all tested concentrations of MGC without drug loading (Fig. 7C(a)), since the cell growth rates with MGC are the same as that of the medium control, proving that the conjugation of β-CD has greatly reduce cytotoxicity and enhance the biocompatibility of the nanocarrier. It can draw a conclusion that MGC is biocompatible and efficient to provide a probable secure vehicle for drug delivery and cancer therapy.

4. Conclusions

In summary, β-CD functionalized graphene oxide-magnetic nanocomposite is successfully constructed by an efficient layer-by-layer assembly method, which could be firstly served as nanocarrier for targeted delivery of stereoisomeric anticancer drugs, DOX and EPI. The MGC5 containing the most β-CD (21.18%) shows higher loading capacity for DOX (909.09 mg/g)

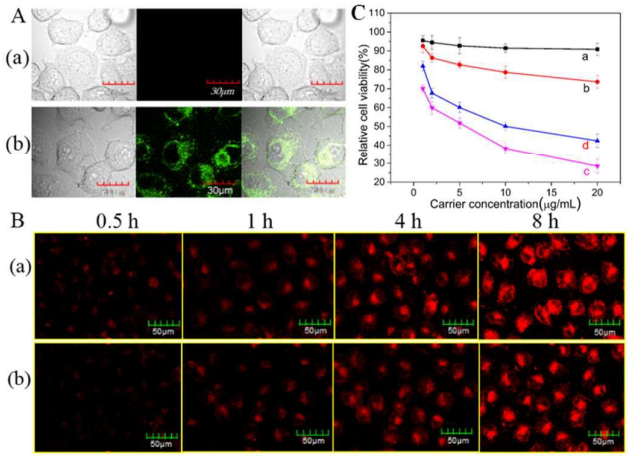

Fig. 7 (A) CLSM images of MCF-7 cells incubated with 20 μg/mL MGC (a) and MGC/FITC (b) at 37 °C for 2 h, respectively. (left) bright-field image; (middle) dark-field image; (right) merged image. The excitation wavelength was 485 nm and the emission was collected at 590 nm (FV1000 CLSM, 60 objective lens). (B) CLSM images of MCF-7 cells after incubation with MGC/DOX (a) and MGC/EPI (b) for incubation time of 0.5h, 1 h, 4 h and 8 h (FV1000 CLSM, 20 objective lens). (C) Relative cellular viability of MCF-7 cells after treatment with various concentrations of MGC (a), MG (b), MGC/DOX (c) and MGC/EPI (d).

than EPI (781.25 mg/g), owing to the formation of different complex constructions with β-CD. The MGC can be internalized into the cell cytoplasm rapidly, and more DOX than EPI could be efficiently released from MGC in acidic cytoplasm of cancer cells based on the pH-dependent accelerated release. The DOX loaded MGC reveals a remarkably higher potency to kill MCF-7 cells than that of EPI, while the blank MGC shows no cytotoxicity. Therefore, the MGC nanohybrid could be an excellent candidate for targeted delivery of stereoisomeric anticancer drugs for biomedical applications.

Acknowledgments

This work was financed by the National Natural Foundations of China (No.21175087 and No.21175086), Shanxi Scholarship Council of China and International Science and Technology Cooperation Program of China (2012DFA207705). Special thanks to Dr Yue Yu's patient guidance and help in AFM images of the national center for nanoscience and technology.

References

1. Y. Gao, Y. Li, X. Zou, H. Huang and X. Su, *Analytica Chimica Acta*, 2012, **731**, 68-74.
2. Y. Guo, L. Deng, J. Li, S. Guo, E. Wang and S. Dong, *ACS Nano*, 2011, **5**, 1282-1290.
3. L. L. Zhang, Z. Xiong and X. S. Zhao, *ACS Nano*, 2010, **4**, 7030-7036.
4. H. Bao, Y. Pan, Y. Ping, N. G. Sahoo, T. Wu, L. Li, J. Li and L. H. Gan, *Small*, 2011, **7**, 1569-1578.
5. Y. Hu, F. Li, X. Bai, D. Li, S. Hua, K. Wang and L. Niu, *Chemical Communications*, 2011, **47**, 1743-1745.
6. M. Liu, H. Zhao, X. Quan, S. Chen and X. Fan, *Chemical Communications*, 2010, **46**, 7909-7911.

7. C. Peng, W. Hu, Y. Zhou, C. Fan and Q. Huang, *Small*, 2010, **6**, 1686-1692.
8. D. Depan, B. Girase, J. S. Shah and R. D. K. Misra, *Acta Biomaterialia*, 2011, **7**, 3432-3445.
9. Z. Liu, J. T. Robinson, X. Sun and H. Dai, *Journal of the American Chemical Society*, 2008, **130**, 10876-10877.
10. X. Yang, Y. Wang, X. Huang, Y. Ma, Y. Huang, R. Yang, H. Duan and Y. Chen, *Journal of Materials Chemistry*, 2011, **21**, 3448-3454.
11. C. X. Guo, H. B. Yang, Z. M. Sheng, Z. S. Lu, Q. L. Song and C. M. Li, *Angewandte Chemie International Edition*, 2010, **49**, 3014-3017.
12. C. N. R. Rao, A. K. Sood, K. S. Subrahmanyam and A. Govindaraj, *Angewandte Chemie International Edition*, 2009, **48**, 7752-7777.
13. X. Sun, Z. Liu, K. Welsher, J. Robinson, A. Goodwin, S. Zaric and H. Dai, *Nano Res.*, 2008, **1**, 203-212.
14. M. Guo, Y. Yan, H. Zhang, H. Yan, Y. Cao, K. Liu, S. Wan, J. Huang and W. Yue, *Journal of Materials Chemistry*, 2008, **18**, 5104-5112.
15. C. Xu, X. Wang, J. Zhu, X. Yang and L. Lu, *Journal of Materials Chemistry*, 2008, **18**, 5625-5629.
16. S. Chen, L. Brown, M. Levendorf, W. Cai, S.-Y. Ju, J. Edgeworth, X. Li, C. W. Magnuson, A. Velamakanni, R. D. Piner, J. Kang, J. Park and R. S. Ruoff, *ACS Nano*, 2011, **5**, 1321-1327.
17. P. K. S. Mural, S. P. Pawar, S. Jayanthi, G. Madras, A. K. Sood and S. Bose, *ACS Appl. Mater. Interfaces*, 2015, **7**, 16266-16278.
18. N. Pamme and A. Manz, *Analytical Chemistry*, 2004, **76**, 7250-7256.
19. G. Xie, P. Xi, H. Liu, F. Chen, L. Huang, Y. Shi, F. Hou, Z. Zeng, C. Shao and J. Wang, *Journal of Materials Chemistry*, 2012, **22**, 1033-1039.
20. X. Yang, X. Zhang, Y. Ma, Y. Huang, Y. Wang and Y. Chen, *Journal of Materials Chemistry*, 2009, **19**, 2710-2714.
21. X. Ma, H. Tao, K. Yang, L. Feng, L. Cheng, X. Shi, Y. Li, L. Guo and Z. Liu, *Nano Res.*, 2012, **5**, 199-212.
22. C. Wang, S. Ravi, U. S. Garapati, M. Das, M. Howell, J. Mallela, S. Alwarappan, S. S. Mohapatra and S. Mohapatra, *J. Mater. Chem. B*, 2013, **1**, 4396-4405.
23. L. Yan, Y.-N. Chang, L. Zhao, Z. Gu, X. Liu, G. Tian, L. Zhou, W. Ren, S. Jin, W. Yin, H. Chang, G. Xing, X. Gao and Y. Zhao, *Carbon*, 2013, **57**, 120-129.
24. G. Xu, P. Xu, D. Shi and M. Chen, *RSC Adv.*, 2014, **4**, 28807-28813.
25. R.-P. Liang, C.-M. Liu, X.-Y. Meng, J.-W. Wang and J.-D. Qiu, *J. Chromatogr. A*, 2012, **1266**, 95-102.
26. X. Liu, L. Yan, W. Yin, L. Zhou, G. Tian, J. Shi, Z. Yang, D. Xiao, Z. Gu and Y. Zhao, *J. Mater. Chem. A*, 2014, **2**, 12296-12303.
27. X.-j. Hu, Y.-g. Liu, H. Wang, G.-m. Zeng, X. Hu, Y.-m. Guo, T.-t. Li, A.-w. Chen, L.-h. Jiang and F.-y. Guo, *Chem. Eng. Res. Des.*, 2015, **93**, 675-683.
28. R. L. Momparier, M. Karon, S. E. Siegel and F. Avila, *Cancer Res.*, 1976, **36**, 2891-2895.
29. J. You, G. Zhang and C. Li, *ACS Nano*, 2010, **4**, 1033-1041.
30. W. S. Hummers, Jr. and R. E. Offeman, *J. Am. Chem. Soc.*, 1958, **80**, 1339.
31. Y. Guo, S. Guo, J. Ren, Y. Zhai, S. Dong and E. Wang, *ACS Nano*, 2010, **4**, 4001-4010.
32. L. Li, L. Fan, M. Sun, H. Qiu, X. Li, H. Duan and C. Luo, *Int. J. Biol. Macromol.*, 2013, **58**, 169-175.
33. A. S. Luebbe, C. Bergemann, W. Huhnt, T. Fricke, H. Riess, J. W. Brock and D. Huhn, *Cancer Res.*, 1996, **56**, 4694-4701.
34. J. Shen, Y. Hu, M. Shi, N. Li, H. Ma and M. Ye, *J. Phys. Chem. C*, 2010, **114**, 1498-1503.
35. Y. Zhu, S. Murali, W. Cai, X. Li, J. W. Suk, J. R. Potts and R. S. Ruoff, *Adv. Mater. (Weinheim, Ger.)*, 2010, **22**, 3906-3924.
36. Y. Tian, B. Yu, X. Li and K. Li, *Journal of Materials Chemistry*, 2011, **21**, 2476-2481.
37. Z. Liu, J. Wang, D. Xie and G. Chen, *Small*, 2008, **4**, 462-466.
38. M. Tabuchi, K. Ado, H. Kobayashi, I. Matsubara, H. Kageyama, M. Wakita, S. Tsutsui, S. Nasu, Y. Takeda, C. Masquelier, A. Hirano and R. Kanno, *Journal of Solid State Chemistry*, 1998, **141**, 554-561.
39. C. Zhu, S. Guo, Y. Fang and S. Dong, *ACS Nano*, 2010, **4**, 2429-2437.
40. L. Zhang, J. Xia, Q. Zhao, L. Liu and Z. Zhang, *Small*, 2010, **6**, 537-544.
41. S. Lv, M. Zhao, C. Cheng and Z. Zhao, *Journal of Nanoparticle Research*, 2014, **16**, 1-12.
42. H. Pandey, V. Parashar, R. Parashar, R. Prakash, P. W. Ramteke and A. C. Pandey, *Nanoscale*, 2011, **3**, 4104-4108.
43. M. Yang, L.-Y. Chu, R. Xie and C. Wang, *Macromolecular Chemistry and Physics*, 2008, **209**, 204-211.
44. X. Fan, G. Jiao, W. Zhao, P. Jin and X. Li, *Nanoscale*, 2013, **5**, 1143-1152.
45. Z. Cao, X. Yue, X. Li and Z. Dai, *Langmuir*, 2013, **29**, 14976-14983.
46. T. Jiang, Z. Zhang, Y. Zhang, H. Lv, J. Zhou, C. Li, L. Hou and Q. Zhang, *Biomaterials*, 2012, **33**, 9246-9258.
47. Y.-J. Lu, K.-C. Wei, C.-C. M. Ma, S.-Y. Yang and J.-P. Chen, *Colloids Surf., B*, 2012, **89**, 1-9.
48. N. W. S. Kam, Z. Liu and H. Dai, *Angewandte Chemie International Edition*, 2006, **45**, 577-581.
49. Z. Luo, K. Cai, Y. Hu, J. Li, X. Ding, B. Zhang, D. Xu, W. Yang and P. Liu, *Advanced Materials*, 2012, **24**, 431-435.
50. K. Hayashi, K. Ono, H. Suzuki, M. Sawada, M. Moriya, W. Sakamoto and T. Yogo, *ACS Applied Materials & Interfaces*, 2010, **2**, 1903-1911.
51. S. Lv, Y. Song, Y. Song, Z. Zhao and C. Cheng, *Applied Surface Science*, 2014, **305**, 747-752.
52. J. V. Jokerst, T. Lobovkina, R. N. Zare and S. S. Gambhir, *Nanomedicine (London, U. K.)*, 2011, **6**, 715-728.
53. H. Xu, L. Cheng, C. Wang, X. Ma, Y. Li and Z. Liu, *Biomaterials*, 2011, **32**, 9364-9373.

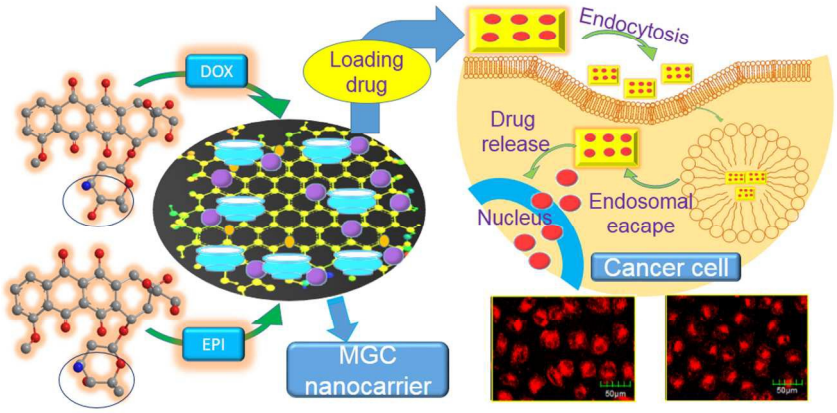

338x190mm (96 x 96 DPI)